

# Evolution of spherical overdensities in holographic dark energy models

Tayebe Naderi,<sup>1</sup> Mohammad Malekjani<sup>1★</sup> and Francesco Pace<sup>2,3</sup>

<sup>1</sup>*Department of Physics, Bu-Ali Sina University, Hamedan 65178, Iran*

<sup>2</sup>*Jodrell Bank Centre for Astrophysics, School of Physics and Astronomy, The University of Manchester, Manchester M13 9PL, UK*

<sup>3</sup>*Institute of Cosmology and Gravitation, University of Portsmouth, Dennis Sciana Building, Portsmouth PO1 3FX, UK*

Accepted 2014 November 23. Received 2014 November 20; in original form 2014 August 25

## ABSTRACT

In this work, we investigate the spherical collapse model in flat Friedmann–Robertson–Walker (FRW) dark energy universes. We consider the holographic dark energy (HDE) model as a dynamical dark energy scenario with a slowly time-varying equation-of-state parameter  $w_{de}$  in order to evaluate the effects of the dark energy component on structure formation in the universe. We first calculate the evolution of density perturbations in the linear regime for both phantom and quintessence behaviour of the HDE model and compare the results with standard Einstein–de Sitter and  $\Lambda$  cold dark matter ( $\Lambda$ CDM) models. We then calculate the evolution of two characterizing parameters in the spherical collapse model, i.e. the linear density threshold  $\delta_c$  and the virial overdensity parameter  $\Delta_{vir}$ . We show that in HDE cosmologies the growth factor  $g(a)$  and the linear overdensity parameter  $\delta_c$  fall behind the values for a  $\Lambda$ CDM universe while the virial overdensity  $\Delta_{vir}$  is larger in HDE models than in the  $\Lambda$ CDM model. We also show that the ratio between the radius of the spherical perturbations at the virialization and turn-around time is smaller in HDE cosmologies than that predicted in a  $\Lambda$ CDM universe. Hence, the growth of structures starts earlier in HDE models than in  $\Lambda$ CDM cosmologies and more concentrated objects can form in this case. It has been shown that the non-vanishing surface pressure leads to smaller virial radius and larger virial overdensity  $\Delta_{vir}$ . We compare the predicted number of haloes in HDE cosmologies and find out that in general this value is smaller than for  $\Lambda$ CDM models at higher redshifts and we compare different mass function prescriptions. Finally, we compare the results of the HDE models with observations.

**Key words:** methods: analytical – cosmology: theory – dark energy.

## 1 INTRODUCTION

Cosmic structures such as galaxies and galaxy clusters develop from the gravitational collapse (Gunn & Gott 1972; Press & Schechter 1974; White & Rees 1978; Peebles 1993; Peacock 1999; Sheth & Tormen 1999; Barkana & Loeb 2001; Peebles & Ratra 2003; Ciardi & Ferrara 2005; Bromm & Yoshida 2011) of primeval small density perturbations originated during the inflationary era (Starobinsky 1980; Guth 1981; Linde 1990). To study the non-linear evolution of cosmic structures, a popular analytical model, the spherical collapse model, was first introduced by Gunn & Gott (1972) and extended and improved by several following works (Fillmore & Goldreich 1984; Bertschinger 1985; Hoffman & Shaham 1985; Ryden & Gunn 1987; Avila-Reese, Firmani & Hernández 1998; Subramanian, Cen & Ostriker 2000; Ascasibar et al. 2004; Williams, Babul & Dalcanton 2004). Recently, the formalism of the spherical collapse model was extended to include shear and rotation (del Popolo, Pace &

Lima 2013a,b,c) and non-minimally coupled models (Pace et al. 2014). In the spherical collapse model, at early times primordial spherical overdense regions expand along the Hubble flow, and since the relative overdensity of the overdense region with respect to the background is small, the linear theory is able to follow their evolution. At a certain point, gravity starts dominating and opposes the expansion slowing it down till the sphere reaches a maximum radius and completely detaches from the background expansion. The following phase is represented by the collapse of the sphere under its own self-gravity. In the approximations introduced by the model, the collapse ends only when the final radius becomes null. This is obviously not the case with real structures, as virialization takes place thanks to non-linear processes converting the kinetic energy of collapse into random motions. The exact process of collapse due to gravitational instability depends strongly on the dynamics of the background Hubble flow.

In the last two decades, the astronomical data from SNe Ia (Riess et al. 1998, 2004, 2007; Perlmutter et al. 1999), CMB (Jaffe et al. 2001; Ho et al. 2008; Jarosik et al. 2011; Komatsu et al. 2011; Planck Collaboration XV 2014; Planck Collaboration XVI 2014;

\*E-mail: [malekjani@basu.ac.ir](mailto:malekjani@basu.ac.ir)

Planck Collaboration XIX 2014), large-scale structure and baryon acoustic oscillations (BAO; Tegmark et al. 2004; Eisenstein et al. 2005; Percival et al. 2010) and X-ray (Allen et al. 2004; Vikhlinin et al. 2009) experiments indicate that the universe is expanding at an accelerated rate. In the framework of General Relativity (GR), an exotic component with positive density and negative pressure, the so-called dark energy (DE), is responsible for this accelerated expansion. Results of the *Planck* experiment (Planck Collaboration XVI 2014) show that DE occupies about 68 per cent, dark matter about 27 per cent and usual baryons occupy about 5 per cent of the total energy budget of the universe.

DE not only affects the expansion rate of the background Hubble flow and the distance–redshift relation, but also the scenario of structure formation. The main goal of this work is to study the effect of DE on structure formation within the spherical collapse model framework.

The first and simplest model for DE is Einstein’s cosmological constant with constant equation-of-state (EoS) parameter  $w_\Lambda = -1$ . For the cosmological constant, structure growth, both in linear and non-linear regimes, has been discussed by Lahav et al. (1991), Lilje (1992), Lacey & Cole (1993), Eke, Cole & Frenk (1996), Viana & Liddle (1996), Kulinich & Novosyadlyj (2003), Debnath, Nath & Chakraborty (2006), Meyer, Pace & Bartelmann (2012). However, the cosmological constant suffers from the fine-tuning and cosmic coincidence problems (Weinberg 1989; Sahni & Starobinsky 2000; Carroll 2001; Padmanabhan 2003; Peebles & Ratra 2003; Copeland, Sami & Tsujikawa 2006). Structure growth has been also investigated in quintessence models with constant EoS parameter different from  $-1$ . In quintessence models, the principal difference is that the energy density decreases with time, whereas for the cosmological constant it remains constant throughout the cosmic history. For constant EoS parameters in the range  $-1 < w_\Lambda < -1/3$ , Horellou & Berge (2005) showed that structures form earlier and are more concentrated in quintessence than in  $\Lambda$  cold dark matter ( $\Lambda$ CDM) models. In addition, the evolution of structure growth and cluster abundance in quintessence DE models (Wang & Steinhardt 1998; Lokas 2001; Basilakos 2003; Mota & van de Bruck 2004) and chameleon scalar field (Brax, Rosenfeld & Steer 2010) have been investigated. It has also been shown that predictions of the spherical collapse model strongly depend on the scalar field potential adopted in a minimally coupled scalar field scenario (Mota & van de Bruck 2004). When DE clusters, Basilakos, Sanchez & Perivolaropoulos (2009), Basilakos, Plionis & Solà (2010) showed that more concentrated structures can be formed with respect to a homogeneous DE model. Bartelmann, Doran & Wetterich (2006) and Pace, Waizmann & Bartelmann (2010) extended the spherical collapse model in the presence of early DE models and showed that the growth of structures is slowed down with respect to the  $\Lambda$ CDM model. Hence, to reach the same amplitude of fluctuations today, the structures have to grow earlier in this type of models.

On the other hand, in recent years, a wealth of dynamical DE models with a time-varying EoS has been proposed (Copeland et al. 2006; Li et al. 2011; Bamba et al. 2012). Observationally, the latest astronomical data from SNe Ia, CMB and BAO experiments show that dynamical DE models with time-varying EoS parameter are mildly favoured (Alam, Sahni & Starobinsky 2004; Gong 2005; Gong & Zhang 2005; Huterer & Cooray 2005; Wang & Tegmark 2005; Zhao et al. 2012). The holographic dark energy (HDE) model (see Section 2 for a complete description of the model) is one of the most interesting proposal in the category of dynamical DE scenarios. In this work, we study the evolution of spherical overdensities in HDE models. The HDE model is considered as a dynamical DE

model with time-varying EoS parameter which can dominate the Hubble flow and influence the growth of structures in the Universe. Here, we consider the non-interacting case of HDE model. In this case, DE is minimally coupled to dark matter and the energy density of DE and dark matter is conserved separately. Therefore, in non-interacting HDE models, we assume a uniform distribution of DE inside the perturbed region. In this case, the energy density of DE remains the same both inside and outside the overdense region. However, in the case of interacting models, the energy density of dark matter and DE is not conserved separately and their coupling is non-minimal. Hence, the DE component can cluster in a similar fashion as dark matter does.

The plan of the paper is the following. In Section 2, we present HDE cosmologies. In Section 3, we discuss the linear evolution of perturbations in HDE cosmology and in Section 4 we study the non-linear spherical collapse model. In Section 5, numerical results and comparison with observations have been presented. Finally, we conclude in Section 6.

## 2 COSMOLOGY WITH HDE

The HDE model is constructed based on the holographic principle in quantum gravity scenario (Susskind 1995). While almost all dynamical DE models with time-varying EoS are purely phenomenological (there is no theoretically motivated model behind them), the advantage of the HDE model is that it originates from a fundamental principle in quantum gravity, therefore possesses some features of an underlying theory of DE. According to the holographic principle, the number of degrees of freedom of a finite-size system should be finite and bounded by the area of its boundary (Cohen, Kaplan & Nelson 1999). In this case, the total energy of a system with size  $L$  should not exceed the mass of a black hole with same size, i.e.  $L^3 \rho_\Lambda \leq LM_{\text{Pl}}^2$ , where  $\rho_\Lambda$  is the quantum zero-point energy density caused by UV cut-off  $\Lambda$  and  $M_{\text{Pl}}$  is the Planck mass ( $M_{\text{Pl}} = 1/8\pi G$ ). In a cosmological context, when the whole Universe is taken into account, the vacuum energy related to the holographic principle is viewed as DE, the so-called HDE. The largest IR cut-off  $L$  is chosen by turning the previous inequality into an equality, hence the following equation is taken for DE density in holographic models:

$$\rho_{\text{de}} = 3c^2 M_{\text{Pl}}^2 L^{-2}, \quad (1)$$

where  $c$  is a positive numerical constant and the coefficient 3 is just for convenience. An interesting feature of HDE is that it has a close connection with the space–time (Ng 2001; Arzano, Kephart & Ng 2007).

From an observational point of view, HDE models have been constrained by various astronomical observations (Alam et al. 2004; Huang & Gong 2004; Zhang & Wu 2005; Wu et al. 2008; Ma, Gong & Chen 2009). Using recent observational data, the value of the holographic parameter  $c$  in a flat Universe was constrained to  $c = 0.815^{+0.179}_{-0.139}$  (Enqvist & Sloth 2004; Gong 2004; Huang & Gong 2004; Huang & Li 2004; Li et al. 2009). The cosmic coincidence problem can be solved by inflation in HDE model (Li 2004).

It should be noted that the HDE model is defined by assuming an IR cut-off  $L$  in equation (1). The simplest choice for IR cut-off is the Hubble length,  $L = H^{-1}$ . If we take  $L$  as the Hubble scale  $H^{-1}$ , DE density will be close to the observational data. However, in this case we get a wrong EoS for HDE models and the current accelerated expansion of the Universe cannot be recovered (Hořava & Minic 2000; Cataldo et al. 2001; Thomas 2002; Hsu 2004). Another choice for the IR cut-off is the particle horizon, which however does not lead to the current accelerated expansion (Hořava & Minic 2000;

Cataldo et al. 2001; Thomas 2002; Hsu 2004). The third choice for the IR cut-off is the future event horizon which was first assumed by Li (2004) for HDE models. The event horizon is given by

$$R_h = a \int_t^\infty \frac{dt}{a(t)} = a \int_t^\infty \frac{da}{Ha(t)}, \quad (2)$$

where  $a$  is the scale factor and  $t$  is cosmic time. In the context of the event horizon, the HDE model can generate the late-time acceleration consistently with observations (Pavón & Zimdahl 2005; Zimdahl & Pavón 2007; Sheykhi 2011). The coincidence and fine-tuning problems are also solved in this case (Li 2004). In fact, a time-varying DE model results in a better fit compared with the standard cosmological constant based on analysis of cosmological data of Type Ia supernova (Alam et al. 2004; Gong 2005; Gong & Zhang 2005; Huterer & Cooray 2005; Wang & Tegmark 2005).

The dynamics of a flat Friedmann–Robertson–Walker (FRW) Universe containing pressureless dark matter and DE components is given by Friedmann equation as follows:

$$H^2 = \frac{1}{3M_{\text{Pl}}^2}(\rho_m + \rho_{\text{de}}), \quad (3)$$

where  $\rho_m$  and  $\rho_{\text{de}}$  are the energy density of the pressureless matter and DE components, respectively, and  $H$  is the Hubble parameter. Here, we use equation (1) for the energy density of DE. For non-interacting DE models, the energy density of DE and dark matter is given by the following continuity equations:

$$\dot{\rho}_m + 3H\rho_m = 0, \quad (4)$$

$$\dot{\rho}_{\text{de}} + 3H(1 + w_{\text{de}})\rho_{\text{de}} = 0, \quad (5)$$

where the dot is the derivative with respect to cosmic time and  $w_{\text{de}}$  is the EoS parameter of DE.

Taking the time derivative of Friedmann equation (3) and using equations (4) and (5), the relation  $\dot{R}_h = 1 + HR_h$  and also the expression for the energy density of HDE models  $\rho_{\text{de}} = 3c^2 M_{\text{Pl}}^2 R_h^{-2}$ , the EoS parameter of the HDE model is

$$w_{\text{de}} = -\frac{1}{3} - \frac{2\sqrt{\Omega_{\text{de}}}}{3c}, \quad (6)$$

where  $\Omega_{\text{de}}$  is the dimensionless density parameter of the DE component.

At late times, when DE dominates the energy budget of the Universe ( $\Omega_{\text{de}} \rightarrow 1$ ), we obtain  $w_{\text{de}} < -1$  for  $c < 1$ . In this case, the EoS parameter of the HDE model is in the phantom regime ( $w_{\text{de}} < -1$ ). For  $c \geq 1$ , we get  $-1 \leq w_{\text{de}} < -1/3$ , indicating the quintessence regime. The analysis of the properties of DE from some recent observations favour models with  $w_{\text{de}}$  crossing  $-1$  in the near past (Alam et al. 2004; Gong 2005; Gong & Zhang 2005; Huterer & Cooray 2005; Wang & Tegmark 2005; Zhao et al. 2012). The evolution of the DE density parameter  $\Omega_{\text{de}}$  in HDE models can be obtained by taking the time derivative of  $\Omega_{\text{de}} = \rho_{\text{de}}/\rho_c = 1/(HR_h)^2$  as follows:

$$\Omega'_{\text{de}} = \Omega_{\text{de}}(1 - \Omega_{\text{de}}) \left( 1 + \frac{2\sqrt{\Omega_{\text{de}}}}{c} \right), \quad (7)$$

where the prime is the derivative with respect to  $x = \ln a$ . Since  $a = 1/(1+z)$ , where  $z$  is the cosmic redshift, we have  $d/dt = Hd/dx = -H(1+z)d/dz$ . In terms of the cosmic redshift, equation (7) is written as

$$\frac{d\Omega_{\text{de}}}{dz} = -\frac{1}{(1+z)}\Omega_{\text{de}}(1 - \Omega_{\text{de}}) \left( 1 + \frac{2\sqrt{\Omega_{\text{de}}}}{c} \right). \quad (8)$$

Also, the differential equation for the evolution of the dimensionless Hubble parameter,  $E(z) = H/H_0$ , in HDE model can be obtained by taking a time derivative of the Friedmann equation (3) and using relations (4)–(6) as follows:

$$\frac{dE}{dz} = -\frac{1}{(1+z)}E \left( \frac{1}{2}\Omega_{\text{de}} + \frac{\Omega_{\text{de}}^{3/2}}{c} - \frac{3}{2} \right). \quad (9)$$

The system of coupled equations (6), (8) and (9) can be solved numerically to obtain the evolution of the EoS parameter, energy density and Hubble parameter in HDE models as a function of cosmic redshift. To fix the cosmology, we assume the present values of matter density and DE density parameters as:  $\Omega_{m,0} = 0.27$  and  $\Omega_{\text{de},0} = 0.73$  in a spatially flat Universe. The present Hubble parameter is  $H_0 = 70 \text{ km s}^{-1} \text{ Mpc}^{-1}$ .

In Fig. 1, we show the evolution of the DE EoS parameter  $w_{\text{de}}$  (top panel), DE density parameter  $\Omega_{\text{de}}$  (middle panel) and dimensionless Hubble parameter  $E = H/H_0$  (bottom panel) as a function of the cosmic redshift  $z$  for three different values of the model parameter  $c$ . We see that for  $c \geq 1$ , the EoS parameter cannot enter into the phantom regime and remains in the quintessence regime. For  $c < 1$ , we adopt the constrained value  $c = 0.815$  from the observational data (Alam et al. 2004). In this case (red-dashed line), the phantom regime can be crossed in the near past in agreement with observations (Alam et al. 2004; Gong 2005; Gong & Zhang 2005; Huterer & Cooray 2005; Wang & Tegmark 2005).

The evolution of  $\Omega_{\text{de}}$  and  $E(z)$  depends on the value of the parameter  $c$ . The Hubble parameter and DE density are bigger in the quintessence regime (green-dotted line).

The cosmic time  $t$  as a function of redshift  $z$  is given by

$$t = \frac{1}{H_0} \int_z^\infty \frac{dz}{(1+z)E(z)}, \quad (10)$$

where  $E(z)$  is the dimensionless Hubble parameter in HDE model. We use equation (10) in order to study the spherical collapse model in HDE cosmologies in Section 4.

### 3 LINEAR PERTURBATION THEORY

Here, we study the linear growth of perturbations of non-relativistic dust matter by calculating the evolution of the growth factor  $g(a)$  in HDE cosmologies and compare it with the solution found for the Einstein–de Sitter (EdS) and  $\Lambda$ CDM models.

For a non-interacting HDE model, we assume that only pressureless matter is perturbed and DE is uniformly distributed. In this case, the differential equation for the evolution of  $g(a)$  is given by (Percival 2005; Pace et al. 2010, 2012)

$$g''(a) + \left( \frac{3}{a} + \frac{E'(a)}{E(a)} \right) g'(a) - \frac{3}{2} \frac{\Omega_{m,0}}{a^5 E^2(a)} g(a) = 0. \quad (11)$$

To obtain the linear growth of structures in HDE cosmologies, we solve numerically equation (11) by using equation (9) for the evolution of the Hubble parameter.

To evaluate the initial conditions, since we are in the linear regime, we assume that the linear growth factor has a power-law solution,  $g(a) \propto a^n$ , with  $n$  to be evaluated at the initial time. We recall that for an EdS model,  $n = 1$ , while in general, in the presence of DE,  $n \neq 1$ . To evaluate the initial slope  $n$ , we insert the power-law solution into the differential equation describing the evolution of the linear growth factor and we solve the second-order algebraic equation obtained.

In Fig. 2, we show the evolution of the linear growth factor  $g(a)$  as a function of the scale factor. We chose to normalize all the

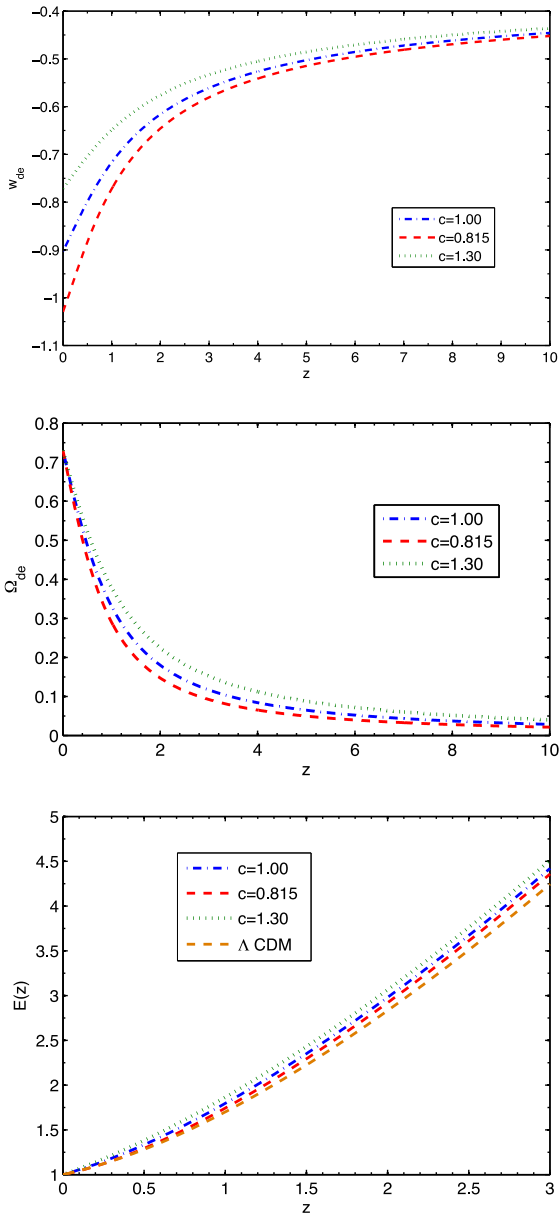


**Figure 1.** Top panel: evolution of the EoS parameter of HDE model  $w_{\text{de}}$  as a function of cosmic redshift  $z$  for different values of the parameter  $c$ . Middle: evolution of the DE density parameter  $\Omega_{\text{de}}$ . Bottom: evolution of the dimensionless Hubble parameter  $E(z) = H/H_0$ . The red-dashed line represents the model with  $c = 0.815$ , the blue dot-dashed curve the model with  $c = 1.00$  and the green-dotted line the model with  $c = 1.30$ . For  $c \geq 1$ , the EoS parameter cannot cross the phantom line  $w = -1$  (quintessence regime). For the constrained value  $c = 0.815$ , the phantom regime is achieved.

models to be the same at early times. We refer to the caption for line style and colours. In the EdS model, the growth factor evolves proportionally to the scale factor, as expected. In the  $\Lambda$ CDM model, the growth factor evolves more slowly compared to the EdS model since at late times the cosmological constant dominates the energy budget of the universe. In the case of HDE model (phantom regime,  $c < 1$ ) with the constrained holographic parameter  $c = 0.815$ ,  $g(a)$  evolves more slowly than in the  $\Lambda$ CDM model. This is due to the fact that the expansion of the Universe considerably slows down structure formation.

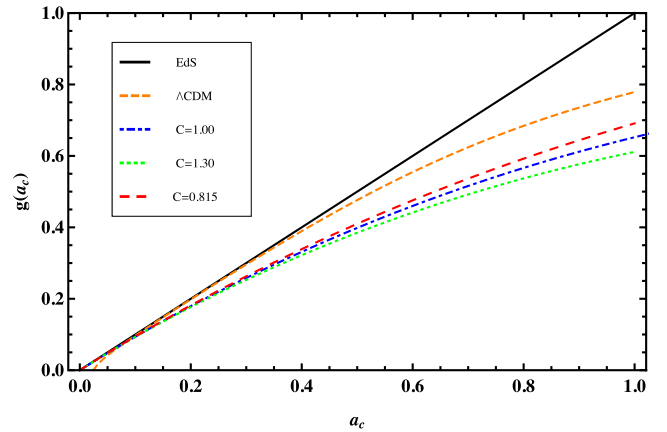


**Figure 2.** Time evolution of the growth factor as a function of the scale factor for the different cosmological models investigated in this work. Black solid line shows the EdS model, the orange short-dashed line the  $\Lambda$ CDM model, the blue (green) dot-dashed (dotted) line the HDE model with  $c = 1.00$  ( $c = 1.30$ ), while the red-dashed line the HDE cosmology with  $c = 0.815$ .

For the quintessence regime ( $c \geq 1$ ), we notice that the evolution of  $g(a)$  is smaller even when compared to the phantom case. This behaviour can be explained by taking into account the evolution of Hubble parameter in Fig. 1. The Hubble parameter is larger in the quintessence regime of the HDE models, it takes intermediate values in the phantom regime and the smallest expansion appears to be in the  $\Lambda$ CDM model. Therefore, the growth factor  $g(a)$  for the HDE will always fall behind the  $\Lambda$ CDM universe.

Here, we conclude that different models for Hubble flow indicate different rate of structure growth in linear regime. In the EdS Universe, in the absence of DE, the growth rate is largest. In the HDE model with  $c = 0.815$ , the growth is the smallest of the models here analysed and it takes intermediate values for the  $\Lambda$ CDM universe. As a result in the linear regime, we see that in HDE models the growth of structures is slowed down compared to  $\Lambda$ CDM and EdS Universes due to bigger Hubble parameter. Hence to have the same fluctuations at the present time, perturbations should start growing earlier in a HDE cosmology than in  $\Lambda$ CDM and EdS scenarios.

#### 4 SPHERICAL COLLAPSE IN HDE MODELS

In this section, we present the spherical collapse model in HDE cosmology. For this purpose, we first review the basic equations we used to derive the correlation between turn-around and virial epochs and then obtain the virial condition in this model. Finally, we obtain the characteristic parameters of the spherical collapse model in the HDE cosmologies.

In the scenario of structure formation, several attempts have been done to obtain the differential equation governing the evolution of the matter perturbation  $\delta$  in the limiting case of a matter-dominated Universe (Bernardeau 1994; Padmanabhan 1996; Ohta, Kayo & Taruya 2003, 2004). In the work of Abramo et al. (2007), the equation for the evolution of  $\delta$  was generalized to a universe containing a DE component with a time-dependent EoS. The differential equation for the evolution of the overdensity  $\delta$  in DE cosmologies and in the presence of rotation and shear tensors has been derived in del Popolo et al. (2013a,c). For the case in which only the dark matter component can cluster, the non-linear differential equation



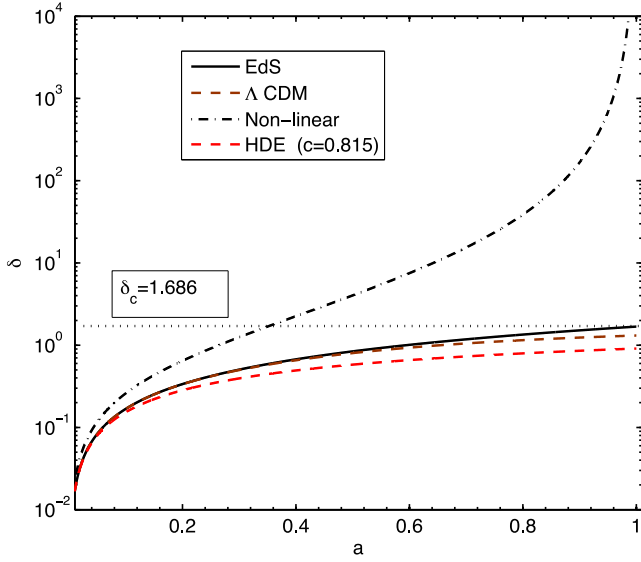


**Figure 3.** The growth of density perturbation  $\delta$  in terms of the scale factor  $a$  for different background models. The black dot–dashed curve stands for non-linear evolution based on equation (12). The black solid line indicates the linear growth of  $\delta$  in CDM model. The brown-dashed one is for the  $\Lambda$ CDM model and the red-dashed curve represents the linear growth of  $\delta$  in the phantom HDE background model.

governing the evolution of  $\delta$  is given by (Pace et al. 2010)

$$\delta'' + \left( \frac{3}{a} + \frac{E'(a)}{E(a)} \right) \delta' - \frac{4}{3} \frac{\delta^2}{1+\delta} - \frac{3}{2} \frac{\Omega_{m,0}}{a^5 E^2(a)} \delta(1+\delta) = 0, \quad (12)$$

where the prime denotes the derivative with respect to the scale factor and  $E$  is the dimensionless Hubble parameter. In the linear regime, the above relation reduces to

$$\delta'' + \left( \frac{3}{a} + \frac{E'(a)}{E(a)} \right) \delta' - \frac{3}{2} \frac{\Omega_{m,0}}{a^5 E^2(a)} \delta = 0. \quad (13)$$

In Fig. 3, the growth of  $\delta$  in the linear and non-linear regimes is presented. To evaluate the initial conditions for the differential equation describing the evolution of perturbations, we refer to Pace et al. (2010) and following the detailed procedure we set initial conditions to  $\delta_i = 2.09 \times 10^{-4}$  and  $\delta'_i = 0$  at the initial scale factor  $a_i = 10^{-4}$ . The black dot–dashed curve represents the solution for  $\delta$  based on non-linear evolution in equation (12) for a collapse time  $a = 1$ . The black solid line is the linear evolution of  $\delta$  for the EdS model according to equation (13). The brown- and red-dashed curves are the linear evolution corresponding to the  $\Lambda$ CDM model and the phantom regime of the HDE cosmology, respectively. We see that the non-linear solution starts to deviate from the linear-based solution and to grow very quickly. In the EdS model,  $\delta$  grows faster and approaches the standard value  $\delta_c = 1.686$  at the collapse scale factor. The linear growth for  $\Lambda$ CDM model is smaller compared to the EdS scenario. In HDE model for  $c = 0.815$ ,  $\delta$  grows more slowly compared to the EdS and  $\Lambda$ CDM models.

#### 4.1 Turn-around and virial redshifts

We know that in the EdS model the time for virialization in the spherical collapse model is twice the turn-around time, i.e.  $t_c = 2t_{ta}$ . Hence, the ratio of the virial to the turn-around scale factor in the EdS Universe is  $a_c/a_{ta} = (t_c/t_{ta})^{2/3} = 2^{2/3} = 1.587$ . Although this

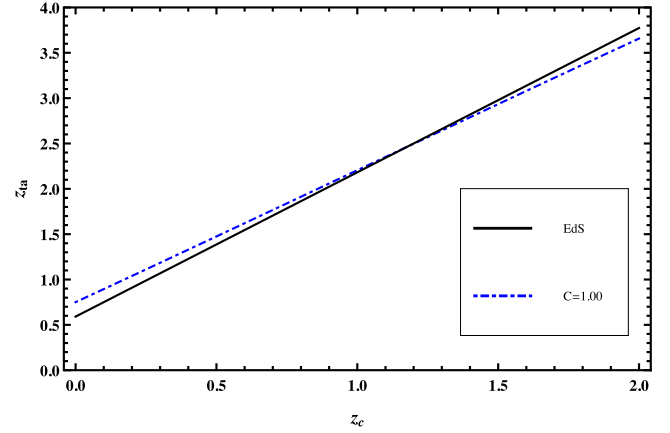


**Figure 4.** The turn-around redshift  $z_{ta}$  in terms of the collapse redshift  $z_c$  for HDE models. The solid curve stands for the EdS model and the dashed one corresponds to the HDE model with holographic parameter  $c = 1$ .

ratio is constant for an EdS Universe, it changes in DE cosmologies. In HDE cosmologies, using equation (10) for the evaluation of the cosmic time, we have

$$\int_{z_c}^{\infty} \frac{dz}{(1+z)E(z)} = 2 \int_{z_{ta}}^{\infty} \frac{dz}{(1+z)E(z)}. \quad (14)$$

By solving the above integrals, we can determine the correlation between turn-around redshift  $z_{ta}$  and collapse redshift  $z_c$ . In Fig. 4, this correlation is shown for an HDE model with holographic parameter  $c = 1$  (blue-dashed line) and EdS model (solid line). Using a linear fitting method, we obtained the following fitting formulas as a correlation between turn-around and collapse redshifts:

$$\begin{aligned} z_{ta} &= 1.542z_c + 0.720, & (c = 1) \\ z_{ta} &= 1.551z_c + 0.728, & (c = 1.3) \\ z_{ta} &= 1.538z_c + 0.713, & (c = 0.815) \\ z_{ta} &= 1.535z_c + 0.740, & (\Lambda\text{CDM}) \\ z_{ta} &= 2^{0.67}(1+z_c) - 1, & (\text{EdS}). \end{aligned} \quad (15)$$

The result for HDE cosmologies is compatible with the fitting formula obtained in  $\Lambda(t)$ CDM cosmology, see equation (34) of Basilakos et al. (2010). As an example, consider a galaxy cluster virializing at the present time  $z_c = 0$ . The turn-around epoch takes place at  $z_{ta} = 0.720$  ( $c = 1$ ),  $z_{ta} = 0.728$  ( $c = 1.3$ ),  $z_{ta} = 0.713$  ( $c = 0.815$ ),  $z_{ta} = 0.740$  ( $w_{de} = -1$ ). It should be noted that in an EdS model the turn-around redshift corresponding to  $z_c = 0$  is  $z_{ta} = 0.591$ . One can conclude that the turn-around epoch takes place earlier for  $\Lambda$ CDM cosmologies, intermediate times are typical of HDE models (by increasing the holographic parameter  $c$ , the turn-around redshift increases accordingly) and later for the EdS Universe. As a further example, consider the virialization process at the higher redshift  $z_c = 1.6$  at which the most distant cluster has been observed (Papovich et al. 2010). In this case, the corresponding turn-around redshift is:  $z_{ta} = 3.187$  ( $c = 1$ ),  $z_{ta} = 3.209$  ( $c = 1.3$ ),  $z_{ta} = 3.173$  ( $c = 0.815$ ),  $z_{ta} = 3.196$  ( $w_{de} = -1$ ) and  $z_{ta} = 3.136$  for the EdS Universe. Here, we see that the turn-around redshift calculated in HDE and  $\Lambda$ CDM models tends to the critical value  $z_{ta} = 3.136$  of the EdS Universe. Therefore at high redshifts, the influence of DE on the virialization process is negligible. This result is expected, because at large redshifts the Universe is dominated by matter and all the models approach the EdS cosmology.

## 4.2 Virial theorem

Here, we investigate the virial theorem in DE cosmologies. The virial theorem relates the kinetic energy  $T$  to a potential energy of the form  $U \propto R^n$  as  $T = (n/2)U$ , where the energies of the system are averaged over time (Landau & Lifshitz 1960; Lahav et al. 1991). In the EdS Universe, the potential energy due to gravitational force is in the form of  $U_G \propto R^{-1}$  and the virial condition is  $2T + U_G = 0$ , where  $T$  is the kinetic energy. In the case of the cosmological constant cosmologies, the virial theorem reads  $2T + U_G = 2U_{de}$ , where  $U_{de}$  is the potential energy due to the DE field (Lahav et al. 1991). The kinetic and potential energies in spherical geometry are given by

$$T = \frac{1}{2} \int u^2 \rho_s dV, \quad (16)$$

$$U_G = -\frac{1}{2} G \iint \frac{\rho_s(r) \rho_s(r')}{|r - r'|} dV dV', \quad (17)$$

$$U_{de} = -\frac{1}{2} G \iint \frac{\rho_s(r) \rho_{de}(r')}{|r - r'|} dV dV', \quad (18)$$

where  $u$  is the peculiar velocity of the fluid element inside the spherical region. For homogeneous DE,  $\rho_{de}$  is uniform inside the collapsing sphere and its dynamics is the same of the background level. Also for a top-hat profile, the distribution of matter inside the spherical collapse is uniform. In this case, for spherical mass fluctuations, the above-mentioned potential energies become

$$U_G = -\frac{16\pi^2 G}{3} \int_0^R r^4 \rho_s^2(r) dr = -\frac{3GM^2}{5R}, \quad (19)$$

$$\begin{aligned} U_{de} &= -\frac{16\pi^2 G}{3} \int_0^R r^4 \rho_s(r) \rho_{de}(r) dr \\ &= -\frac{4\pi G \rho_{de,0} M R^2}{5} (1 + 3w_{de}) e^{3 \int_0^z \frac{1+w_{de}(z)}{1+z} dz}, \end{aligned} \quad (20)$$

where in equation (20) we considered the homogeneous time-varying DE with EoS parameter  $w_{de}(z)$ . Note that in the definition of the potential energy for time-varying HDE field in equation (20), the coefficient  $(1 + 3w_{de})$  leads to a positive DE potential as well, therefore representing a repulsive potential. Thanks to the sign of the coefficient  $(1 + 3w_{de})$ , we do not need to assume the coefficient 2 in the right-hand side of virial theorem defined by Lahav et al. (1991). Also, since the DE potential is considered with positive sign, the virial theorem in this case reads  $2T + U_G + U_{de} = 0$ . For  $w_{de} = -1$ , equation (20) reduces to  $U_{de} = \frac{\Lambda M}{10} R^2$  as in Basilakos et al. (2010).

## 4.3 Spherical collapse parameters

Consider a spherical overdense region with uniform matter density (top-hat profile)  $\rho_s$  and radius  $R$  embedded in a Universe described by its background dynamics elsewhere except for the perturbed region. The dynamics of background follows from Friedmann equation (3). For non-interacting HDE models, DE does not cluster and its energy density  $\rho_{de}$  remains the same both inside and outside the overdense patch. Based on Birkhoff's theorem in GR, the gravitational field inside a spherical symmetric shell should vanish, and this is in agreement with Newtonian gravity. This allows us to use Newtonian dynamics to study the evolution of matter density perturbations on scales much smaller than the horizon. Hence, the

dynamics of the perturbed region is given by

$$\frac{\ddot{R}}{R} = -4\pi G \left( \rho_{de} + \frac{\rho_{de} + \rho_s}{3} \right) = -4\pi G \left[ \left( w_{de} + \frac{1}{3} \right) \rho_{de} + \frac{1}{3} \rho_s \right], \quad (21)$$

where the overdot indicates a derivative with respect to the cosmic time. Here, we use the EoS of DE component to obtain the second equality in equation (21). We know that at early times, when the overdensity of this region is small enough, the expansion of the patch follows the Hubble flow and density perturbations grow (approximately) linearly with the scale factor. With the increase of the density perturbation, the expansion of the perturbed region detaches from the Hubble flow and its expansion velocity decreases. Finally, at a characteristic scale factor  $a_{ta}$ , it completely detaches from the general expansion and starts to collapse under its own gravitational field till virialization takes place. We call  $z_{ta}$  and  $z_c$  the redshifts corresponding to the turn-around and virialization epochs, respectively, and  $R_{ta}$  and  $R_c$  are the corresponding maximum and virial radii, respectively. By defining the dimensionless parameters  $x = a/a_{ta}$  and  $y = R/R_{ta}$ , the evolution of the scale factor of the background and the overdense spherical region (i.e. equations 3 and 21) are governed by the following equations, respectively:

$$\left( \frac{\dot{x}}{x} \right)^2 = H_{ta}^2 \Omega_{mt} \left( x^{-3} + \frac{\rho_{de}}{\rho_{mt}} \right), \quad (22)$$

$$\frac{\ddot{y}}{y} = -\frac{H_{ta}^2 \Omega_{mt}}{2} \left( \frac{\xi}{y^3} + (1 + 3w_{de}) \frac{\rho_{de}}{\rho_{mt}} \right), \quad (23)$$

where  $H_{ta}$ ,  $\rho_{mt}$  and  $\Omega_{mt}$  are the Hubble parameter, the matter density and the matter density parameter at turn-around time, respectively, and  $\xi$  is the ratio of matter density inside the sphere to the matter density at background at turnaround epoch  $\xi = (\rho_s/\rho_m)_{x=1}$ . In order to obtain equation (23), we used the fact that the matter inside the sphere evolves as

$$\rho_s = \rho_{st} \left( \frac{R}{R_{ta}} \right)^{-3} = \frac{\xi \rho_{mt}}{y^3}. \quad (24)$$

We use the following fitting expression obtained by Wang & Steinhardt (1998), Lokas (2001), Basilakos (2003) and Mota & van de Bruck (2004) in the line of *COBE* measurements

$$\xi = \left( \frac{3\pi}{4} \right)^2 \Omega_m^{-0.79+0.26\Omega_m-0.06w_{de}} \Big|_{x=1}. \quad (25)$$

Following Wang & Steinhardt (1998), Lokas (2001), Basilakos (2003) and Mota & van de Bruck (2004), we notice that in equation (25)  $\xi$  is weakly model dependent and can be used for models with time-varying  $w_{de}$ . We apply equation (6) to obtain  $\xi$  in HDE models. In the limiting case of the EdS model,  $\xi = 5.6$  independently of cosmic time. Using the virial theorem for DE cosmology  $2T + U_G + U_{de} = 0$  and the conservation equation between virial and turn-around epochs,  $T_c + U_{G,c} + U_{de,c} = U_{G,t} + U_{de,t}$ , we obtain the following equation for the dimensionless parameter  $\lambda = R_c/R_{ta}$ :

$$\begin{aligned} & \left[ \Omega_{de,0} (1 + 3w_{de}(z_c)) A(z_c) \right] \lambda^3 - 2 \left[ \xi (1 + z_{ta})^3 \Omega_{m,0} \right. \\ & \left. + \Omega_{de,0} (1 + 3w_{de}(z_{ta})) A(z_{ta}) \right] \lambda + \xi (1 + z_{ta})^3 \Omega_{m,0} \\ & = 0, \end{aligned} \quad (26)$$

where we used equations (19) and (20) and define the parameter  $A(z) = e^{3 \int_0^z \frac{1+w_{de}(z')}{1+z'} dz}$ . In the limiting case of an EdS Universe, one can easily see that  $\lambda = 1/2$ , as expected.

In this framework, the overdensity of the collapsing structure at the virialization time is given by

$$\Delta_{\text{vir}} = \frac{\rho_{s,c}}{\rho_{m,c}} = \frac{\xi}{\lambda^3} \left( \frac{1+z_{\text{ta}}}{1+z_c} \right)^3, \quad (27)$$

where  $(1+z_{\text{ta}})/(1+z_c)$ ,  $\xi$  and  $\lambda$  are calculated from equations (15), (25) and (26), respectively. For completeness, we also discuss the parameter  $\delta_c$  defined as the linear evolved primordial perturbations to the collapse epoch. The parameters  $\delta_c$  and  $\Delta_{\text{vir}}$  are the two characterizing parameters in the spherical collapse model. In next section, we present our numerical results for HDE cosmologies and compare them with the concordance  $\Lambda$ CDM model as well as observations.

The framework of the spherical collapse model can be extended to include contributions from the shear and the angular momentum terms in equation (21), in complete analogy with del Popolo et al. (2013c). While an extensive and quantitative analysis of the effects of these two additional non-linear terms goes beyond the purpose of this work, from recent works and based on physical arguments, we can assert that we would expect similar results to previous works, where, due to the additional mass dependence of the spherical collapse parameters, low-mass objects showed higher values for the spherical collapse model parameters  $\delta_c$  and  $\Delta_{\text{vir}}$ , while high-mass objects will be almost completely unaffected. In particular, we expect differences of the order of several percent, based on results by del Popolo et al. (2013c).

#### 4.4 Non-zero surface pressure

In this section, we present a short discussion on the inclusion of the non-vanishing surface pressure term. The surface pressure is due to non-zero density at the outer boundary of virialized clusters. A modified virial relation in the presence of the surface pressure term is given by

$$2T + U_G + U_{\text{de}} = 3P_{\text{ext}}V, \quad (28)$$

where  $P_{\text{ext}}$  is the pressure at the surface of virialized cluster and  $V$  is the volume (Afshordi & Cen 2002; del Popolo 2002). The surface term is related to the total potential energy  $U = U_G + U_{\text{de}}$  as  $3P_{\text{ext}}V = -\nu U$  (Afshordi & Cen 2002). Here, we discuss how the non-vanishing surface pressure can change the spherical collapse parameters. For simplicity, we first assume the standard EdS cosmology. In this case, the modified virial theorem reads  $2T + (1+\nu)U_G = 0$  and the energy conservation between turn-around and virial epochs results in  $\lambda = (1-\nu)/2$ . Hence for  $\nu > 0$ , the parameter  $\lambda$  is smaller than the standard value  $1/2$  and  $\Delta_{\text{vir}}$  will be larger than standard EdS value  $\sim 178$ . For example, for a value  $\nu = 0.005$ , one obtains  $\lambda = 0.04975$  and  $\Delta_{\text{vir}} \simeq 182$  which is 2 percent larger than the standard EdS value. In the general case of an HDE universe, the modified virial theorem can be obtained as  $2T + (1+\nu)(U_G + U_\Lambda) = 0$ . The condition for energy conservation between turn-around and virial epochs,  $T_c + U_{G,c} + U_{\text{de},c} = U_{G,t} + U_{\text{de},t}$ , as well as the modified virial condition lead to the following cubic equation for  $\lambda$ :

$$\begin{aligned} & [(1-\nu)\Omega_{\text{de},0}(1+3w_{\text{de}}(z_c))A(z_c)]\lambda^3 - 2[\xi(1+z_{\text{ta}})^3\Omega_{m,0} \\ & + \Omega_{\text{de},0}(1+3w_{\text{de}}(z_{\text{ta}}))A(z_{\text{ta}})]\lambda \\ & + (1-\nu)\xi(1+z_{\text{ta}})^3\Omega_{m,0} = 0. \end{aligned} \quad (29)$$

Inserting the value  $\nu = 0$ , we recover equation (26) as expected. In the next section, we evaluate the effect of the inclusion of the non-vanishing surface pressure on the spherical collapse parameters  $\lambda$  and  $\Delta_{\text{vir}}$  for the illustrative value  $\nu = 0.005$  and holographic parameter  $c = 1$ .

#### 4.5 Mass function and number density

We now calculate the comoving number density of virialized objects in a given mass range. In the Press–Schechter formalism, the average comoving number density of haloes of mass  $M$  is described by the universal mass function,  $n(M, z)$ :

$$n(M, z) = \left( \frac{\bar{\rho}}{M^2} \right) \frac{d \log \nu}{d \log M} \nu f(\nu), \quad (30)$$

where  $\bar{\rho}$  is the background density and  $f(\nu)$  is the so-called multiplicity function (Press & Schechter 1974; Bond et al. 1991). The variable  $\nu$  is defined as  $\nu = \delta_c^2/\sigma^2(M)$ , where  $\sigma(M)$  is the rms of the mass fluctuation in spheres of mass  $M$ . Since both  $\delta_c$  and  $\sigma(M)$  evolve in time, also the variable  $\nu$  would be in principle a time-dependant function. However, the linear overdensity parameter represents the initial perturbation evolved via the linear growth factor, therefore  $\nu$  is in reality time-independent and probes and initial amplitude of perturbations. In a Gaussian density field,  $\sigma$  is given by

$$\sigma^2(R) = \frac{1}{2\pi^2} \int_0^\infty k^2 P(k) W^2(kR) dk, \quad (31)$$

where  $R = (3M/4\pi\rho_{m0})^{1/3}$  is the radius of the sphere at the present time,  $W(kR) = 3[\sin(kR) - kR\cos(kR)]/(kR)^3$  is the Fourier transform of a spherical top-hat profile with radius  $R$  and  $P(k)$  is the power spectrum of density fluctuations (Peebles 1993). The quantity  $\sigma(M, z)$  can be related to its present value as  $\sigma(M, z) = g(z)\sigma(M, z=0)$ , where  $g(z) = \delta_c(z)/\delta_c(z=0)$  is the linear growth factor. In this work, like Abramo et al. (2007), we use the fitting formula given by Viana & Liddle (1996)

$$\sigma(M, z) = \sigma_8(z) \left( \frac{M}{M_8} \right)^{-\gamma(M)/3}, \quad (32)$$

where  $M_8 = 6 \times 10^{14} \Omega_{m0} h^{-1} M_\odot$  is the mass inside a sphere of radius  $R_8 = 8 h^{-1}$  Mpc,  $\sigma_8$  is the mass variance of the overdensity on the scale of  $R_8$  and the exponent  $\gamma(M)$  depends on the shape parameter  $\Gamma = \Omega_{m0} h \exp(-\Omega_b - \Omega_b/\Omega_{m0})$ . For a spectral index  $n = 1$ , we have

$$\gamma(M) = (0.3\Gamma + 0.2) \left( 2.92 + \frac{1}{3} \log \frac{M}{M_8} \right). \quad (33)$$

Being an approximation, equations (32) and (33) have a limited range of validity and as stated in Viana & Liddle (1996) they match the true shape of  $\sigma_8$  in a region around  $M_8$ . For masses  $M < M_8$  ( $M > M_8$ ), the fitting formula predicts higher (lower) values of the variance, with differences at most of 10 percent. This means that the mass function will predict less (more) objects at lower (higher) masses. This is though not an issue for our analysis, since all the models will be affected in the same way and we are interested in the relative halo abundance.

In order to determine the predicted number density of dark matter haloes for a given cosmological model based on equation (30), we need the mass variance  $\sigma(M, z)$  and multiplicity function  $f(\nu)$ . The standard function  $f(\nu) = \sqrt{2/\pi} e^{-\nu/2}$  provides a good representation of the observed distribution of virialized structures. However, the standard mass function deviates from simulations for low- and high-mass objects. Here, we use another popular fitting formula proposed by Sheth & Tormen (Sheth & Tormen 1999, 2002), the so-called ST mass function:

$$\nu f_{\text{ST}}(\nu) = A_1 \sqrt{\frac{b\nu}{2\pi}} \left(1 + \frac{1}{(b\nu)^p}\right) \exp\left(-\frac{b\nu}{2}\right), \quad (34)$$

where the numerical parameters are:  $A_1 = 0.3222$ ,  $b = 0.707$  and  $p = 0.3$ . For comparison, we also use the following improved mass functions which are, respectively, presented in del Popolo (2006a,b, P06 mass function) and Yahagi, Nagashima & Yoshii (2004, YNY mass function), respectively:

$$\begin{aligned} \nu f(\nu) = A_2 \left[1 + \frac{0.1218}{(b\nu)^{0.585}} + \frac{0.0079}{(b\nu)^{0.4}}\right] \sqrt{\frac{b\nu}{2\pi}} \\ \times \exp\left(-0.4019b\nu \left[1 + \frac{0.5526}{(b\nu)^{0.585}} + \frac{0.02}{(b\nu)^{0.4}}\right]^2\right), \quad (35) \end{aligned}$$

$$\begin{aligned} \nu f(\nu) = A_3 \left[1 + (B\sqrt{\nu/2})^C\right] \nu^{(D/2)} \\ \times \exp\{- (B\sqrt{\nu/2})^2\}, \quad (36) \end{aligned}$$

where  $A_2 = 1.75$ ,  $B = 0.893$ ,  $C = 1.39$  and  $D = 0.408$ , and  $A_3 = 0.298$ .

To determine the mass variance  $\sigma$  via equation (32), we should first calculate  $\sigma_8$ . The present value of  $\sigma_8$  for HDE cosmologies is obtained with

$$\sigma_{8,\text{HDE}} = \frac{\delta_{c,\text{HDE}}(z=0)}{\delta_{c,\Lambda}(z=0)} \sigma_{8,\Lambda}, \quad (37)$$

where  $\sigma_{8,\Lambda} = 0.8$  is the present value of  $\sigma_8$  for the  $\Lambda$ CDM model. The value of  $\sigma_{8,\text{HDE}}$  at redshift  $z$  is therefore obtained as  $\sigma_{8,\text{HDE}}(z) = g(z)\sigma_{8,\text{HDE}}(z=0)$ . Hence, the mass variance  $\sigma(M, z)$  which is required to compute the number density of haloes can be easily obtained from equation (32). In the next section, we present the numerical results of the mass function formalism and number density clusters in HDE cosmologies. We chose this normalization for the DE models studied here so to have approximately the same number of objects at  $z = 0$ . In this way, differences will appear mainly at high redshifts.

## 5 NUMERICAL RESULTS AND COMPARISON WITH OBSERVATION

In this section, we present the numerical results of the spherical collapse model in HDE cosmologies and compare the results with observations. In Fig. 5, the evolution of the linear overdensity threshold parameter  $\delta_c$  is shown as a function of redshift for different models. In the EdS model,  $\delta_c$  is constant and redshift-independent as expected. In the  $\Lambda$ CDM model, the linear overdensity parameter is smaller than the corresponding value for the EdS model at low redshifts and it approaches the standard value of  $\delta_c = 1.686$  at higher redshifts. These two limits are easily explained. At high redshift, the Universe is matter dominated and therefore well described by an EdS model. At low redshift, the cosmological constant dominates, therefore structures must form earlier with a lower critical density.

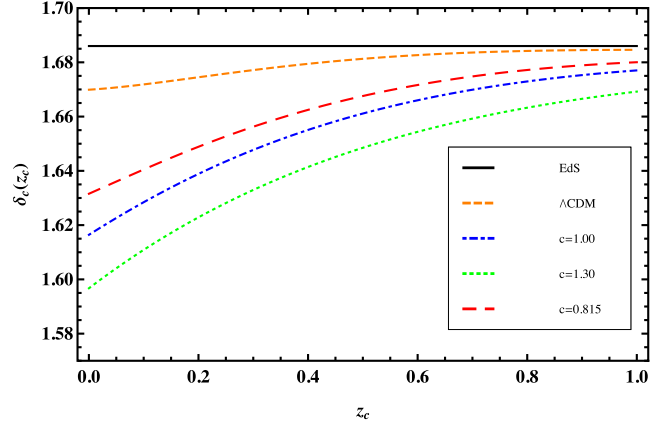


**Figure 5.** The variation of the linear threshold density contrast as a function of the collapse redshift for the different cosmological background models analysed in this work. Line styles and colours are as in Fig. 2.

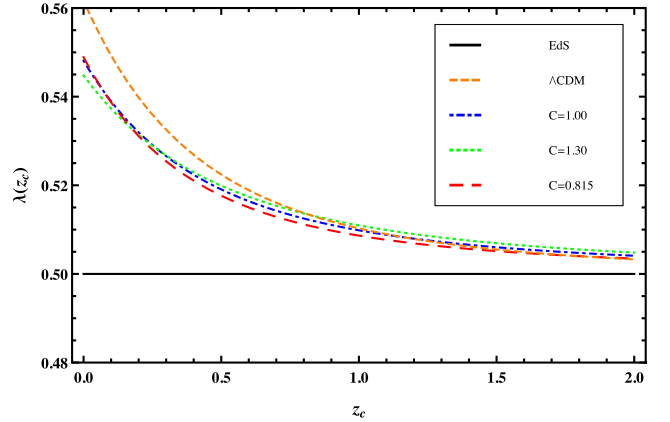


**Figure 6.** Dependence of the dimensionless parameter  $\lambda = R_c/R_{\text{ta}}$  as a function of the collapse redshift  $z_c$  for different cosmological models. Line styles and colours are as in Fig. 2.

In the case of the HDE model (phantom regime) with constrained holographic parameter  $c = 0.815$ ,  $\delta_c$  evolves more slowly than the  $\Lambda$ CDM model. In the quintessence regime ( $c \geq 1$ ), we see that the values of  $\delta_c$  are smaller than the others. These behaviour of  $\delta_c$  is explained by taking into account the evolution of the Hubble parameter in Fig. 1. The Hubble parameter is largest in the quintessence regime of HDE models, it takes intermediate values in the phantom regime in HDE and smallest for  $\Lambda$ CDM model. Therefore, the linear threshold overdensity  $\delta_c$  for the HDE models will always have smaller values than in the  $\Lambda$ CDM universe. Also note that the HDE cosmologies approach the EdS model at high redshifts, even if at a smaller rate than the  $\Lambda$ CDM model.

Now by solving equation (26), we calculate the evolution of the dimensionless parameter  $\lambda = R_c/R_{\text{ta}}$  as a function of collapse redshift  $z_c$ . In Fig. 6, we show  $\lambda$  versus  $z_c$  for the HDE and  $\Lambda$ CDM models. We see that at redshifts large enough, the parameter  $\lambda$  approaches the critical value  $\lambda = 1/2$  indicating once again that at large redshifts matter dominates also in these models and the EdS model is a good approximation. This result is consistent with what found for the linear overdensity parameter  $\delta_c$ . Also note that, as for  $\delta_c$ , the rate of convergence to an EdS model is lower for HDE cosmologies than for a  $\Lambda$ CDM model. We can also conclude



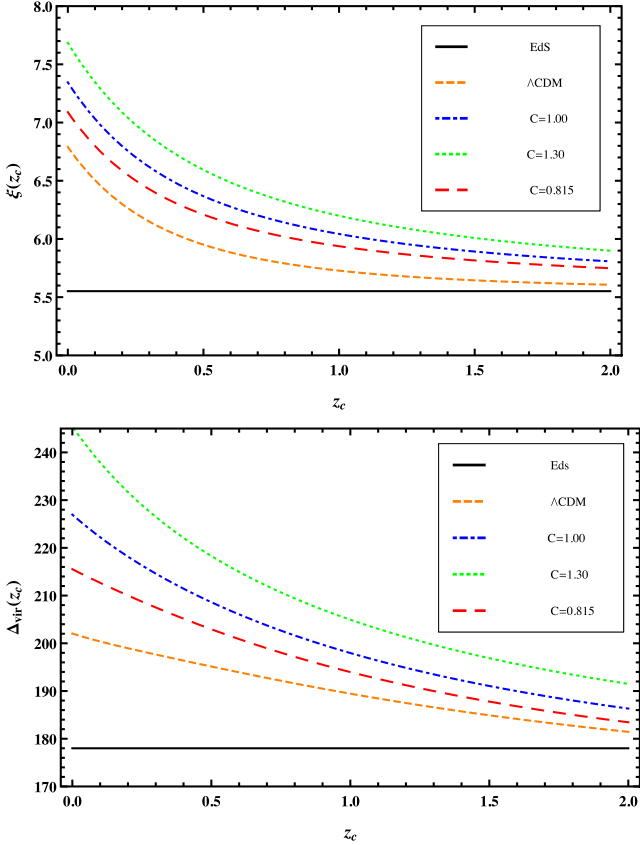


**Figure 7.** The variation of  $\xi$  (top) and virial overdensity  $\Delta_{\text{vir}}$  (down) with collapse redshift  $z_c$  for various models considered in this work. Line styles and colours are as in Fig. 2.

that the size of structures in HDE models (for both phantom and quintessence regimes) are smaller than that predicted by the  $\Lambda$ CDM model ( $\lambda_{\text{HDE}} \leq \lambda_{\Lambda\text{CDM}}$ ).

In Fig. 7, the evolution of the parameter  $\xi$  (top) and of the virial overdensity  $\Delta_{\text{vir}}$  (down) with respect to the collapse redshift  $z_c$  is shown for different models. At early times,  $\xi$  converges to the fiducial value  $\xi \approx 5.6$  which describes the early matter-dominated Universe. Compared to a  $\Lambda$ CDM model, the value of  $\xi$  is larger for both quintessence and phantom regimes of the HDE model. This means that the overdense spherical regions at turn-around are denser in HDE model than in  $\Lambda$ CDM and EdS models. It is also interesting to notice that the overdensity at turn-around  $\xi$  increases monotonically as a function of the free parameter  $c$ . This is easily understood taking into account that with the increase of  $c$ , the model switches from the phantom to the quintessence regime.

We finally discuss the evolution of the virial overdensity parameter  $\Delta_{\text{vir}}$ . This quantity is important for the definition of the halo size. Supposing that haloes can be described approximately with a spherical geometry, its mass  $M_{\text{vir}}$  and radius  $R_{\text{vir}}$  are linked by the following relation:

$$M_{\text{vir}} = \frac{4\pi}{3} \rho_c \Delta_{\text{vir}} R_{\text{vir}}^3, \quad (38)$$

where  $\rho_c$  is the critical density of the Universe. In simulations studies, the critical density is often replaced by the mean background density  $\bar{\rho} = \rho_c \Omega_m$ .

In analogy with what found for the overdensity at turn-around  $\xi$ , we see that the virial overdensity parameter is higher in HDE cosmologies than for the  $\Lambda$ CDM model. Also coherently with

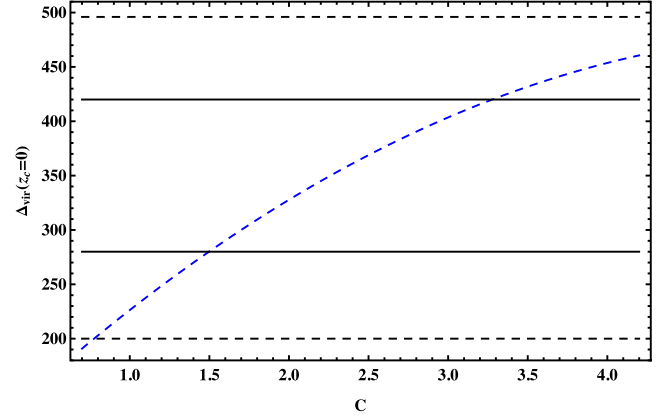


**Figure 8.** The present-time virial overdensity for HDE model as a function of holographic parameter  $c$ . The horizontal solid and dashed lines correspond to the  $1\sigma$  and  $2\sigma$  observational overdensity limits, respectively, based on a subsample of the 2MASS high density contrast group catalogue.

previous results, this quantity increases monotonically increasing the parameter  $c$ . As expected, differences are bigger at small redshifts and gradually decrease at high redshift, where for sufficiently early times all the models will recover the EdS solution,  $\Delta_{\text{vir}} \approx 178$ . Phantom regime gives results closer to what predicted for the  $\Lambda$ CDM cosmology. In this case ( $c = 0.815$ ), differences are of the order of 7 per cent and gradually increase up to more than 20 per cent for  $c = 1.3$ . Intermediate values are found for  $c = 1$ .

We now compare  $\Delta_{\text{vir}}$  calculated in HDE cosmologies with the observational value of the virial overdensity of clusters at the present time  $\Delta_{\text{vir}}^{\text{obs}}(z_c = 0)$ . To do this, we follow the work of Basilakos et al. (2010) in which the present observational value for  $\Delta_{\text{vir}}^{\text{obs}}(z_c = 0)$  with  $1\sigma$  ( $2\sigma$ ) error has been calculated as  $348 \pm 73$  ( $\pm 146$ ) based on a subsample of the 2MASS high density contrast group catalogue (Crook et al. 2007). In Fig. 8, we plot the present-time virial density  $\Delta_{\text{vir}}$  in HDE models as a function of holographic parameter  $c$ . The horizontal solid and dashed lines correspond to the  $1\sigma$  and  $2\sigma$  errors which limit the virial density to  $202 \leq \Delta_{\text{vir}} \leq 494$ . This observational value for the present time sets limits on the value of the holographic parameter to  $0.8 \leq c \leq 4.5$ .

In Fig. 9, we show the effect of the non-vanishing surface pressure at the outer layers of clusters, which appears due to non-zero density at the boundary of clusters, on the spherical collapse parameters  $\lambda$  (top) and  $\Delta_{\text{vir}}$  (down). The blue-dashed (solid brown) curves stand for HDE model with  $c = 1$  without (with) the effect of surface pressure term. When including the surface pressure term, we assume  $\nu = 0.005$ . We see that non-vanishing surface pressure makes the structures to virialize at a smaller radius with respect to standard HDE models. Hence, the virial overdensity  $\Delta_{\text{vir}}$  is higher by assuming surface pressure. Choosing the surface pressure parameter  $\nu = 0.005$ , differences between vanishing and non-vanishing surface pressure HDE model ( $c = 1$ ) for parameter  $\lambda$  and  $\Delta_{\text{vir}}$  at the present-time redshift collapse ( $z_c = 0$ ) are of the order of 1 and 1.5 per cent, respectively. Hence, more denser and compact clusters can be formed when including the effect of surface pressure.

Using equation (37), we obtain  $\sigma_{8,\text{HDE}}(z = 0) = 0.76$  for  $c = 1.3$ ,  $\sigma_{8,\text{HDE}}(z = 0) = 0.77$  for  $c = 1.0$  and  $\sigma_{8,\text{HDE}}(z = 0) = 0.78$  for  $c = 0.815$ . Hence, this quantity increases by decreasing the parameter  $c$ . For  $c = 1.3$ , differences from the  $\Lambda$ CDM value  $\sigma_{8,\Lambda\text{CDM}} = 0.8$  are of the order of 5 per cent and for  $c = 1$  and  $0.815$  are 4 and 2.5 per cent, respectively.

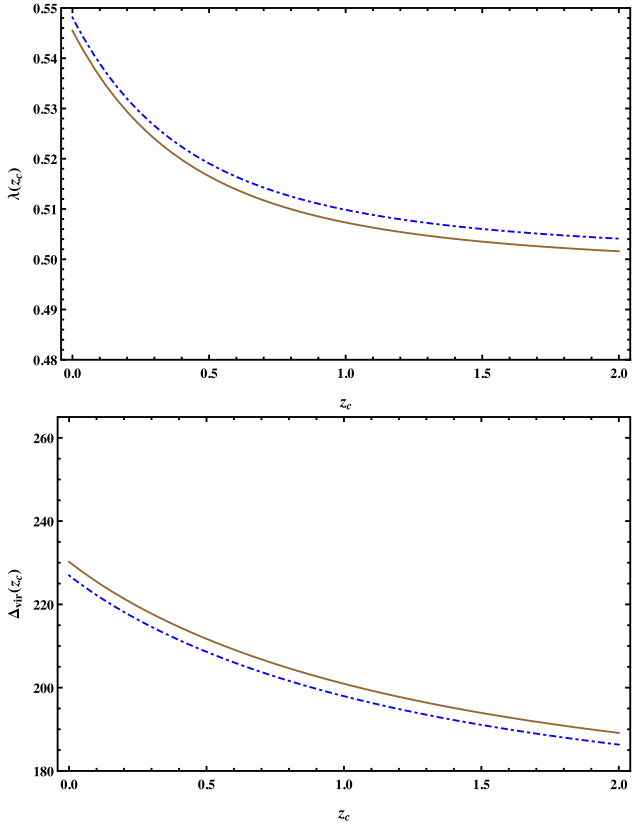


**Figure 9.** The variation of the dimensionless parameter  $\lambda = R_c/R_{\text{ta}}$  (top) and virial overdensity  $\Delta_{\text{vir}}$  (down) as a function of collapse redshift  $z_c$  for HDE model ( $c = 1$ ) with non-vanishing surface pressure (solid brown curve) and zero surface pressure (blue-dashed curve).

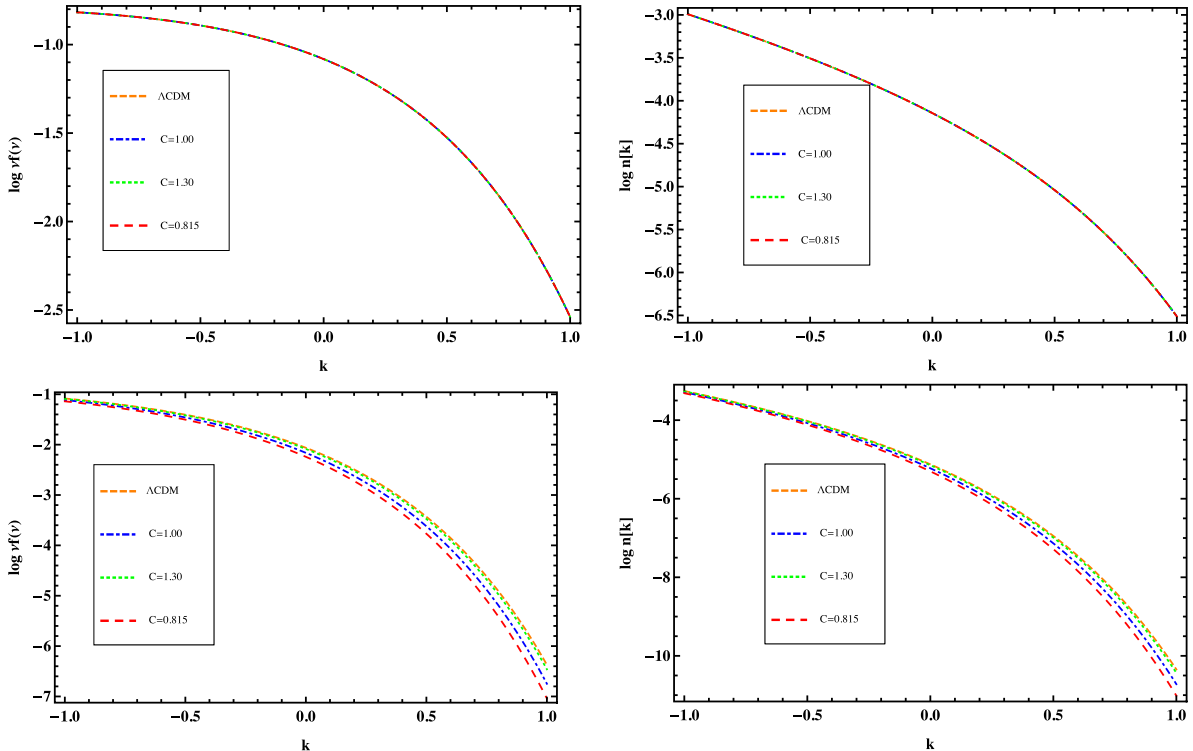


**Figure 10.** Mass function (left-hand panels) and number density (right-hand panels) for HDE and  $\Lambda$ CDM models at present time  $z = 0$  (upper panels) and at  $z = 1$  (lower panels), as described in the legend.

Fig. 10 shows the evolution of the mass function  $v f(v)$  in the upper-left panel and the number density  $n(k)$ , where  $k = \log(M/M_8)$ , in the upper-right panel, as a function of  $k$  for HDE cosmologies as well as  $\Lambda$ CDM at the present time by using the ST mass function in equation (34) proposed by Sheth & Tormen (Sheth & Tormen 1999, 2002). The lower panels show the same quantities, but at  $z = 1$ . Due to the normalization used, the mass function and number density (number of objects above a given mass) are the same for all models at the present time  $z = 0$  and differences appear at high redshifts  $z = 1$ . We also see that the difference of the number densities of halo objects is in the high-mass tail and negligible for small objects (see lower panel). We see in particular that decreasing the free parameter  $c$ , the number of objects per unit mass and volume decreases. For values of  $c > 1$ , the mass function for the HDE model is very similar to the  $\Lambda$ CDM one, differing by it by only 1 per cent. Since for  $c < 1$  we enter in the phantom regime, we expect this model to differ mostly from the  $\Lambda$ CDM one. This is indeed the case as we can see in the lower panels. In this case, differences are of the order of 10 per cent. Intermediate values take place for  $c = 1$  with differences of the order of 6 per cent.

Finally, we compare the results of ST mass function with the improved versions P06 and YNY given in equations (35) and (36), respectively, for HDE cosmologies ( $c = 1$ ). We present our results in Fig. 11. We see that the ST mass function (blue dott-dashed curve) is smaller than P06 (black dot-dashed) and YNY (black-dashed one), for all mass scales. We also see that P06 and YNY are the same for small mass scales and differ at high-mass tail. Differences between the ST and the other mass functions are of the order of 20 per cent, roughly constant throughout the whole mass range investigated.

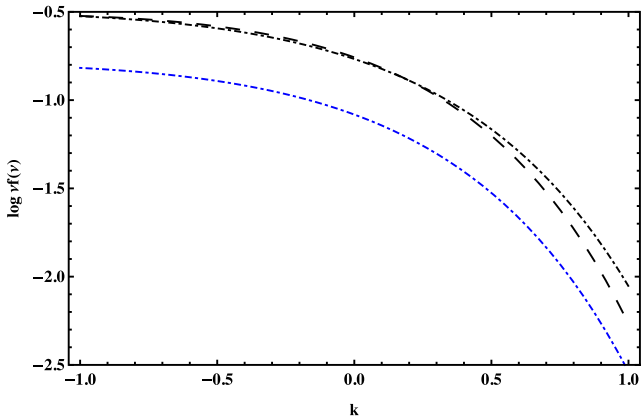


**Figure 11.** Comparing various mass functions considered in this work for HDE model with  $c = 1$ . The blue dotted-dashed curve indicates the ST mass function given by equation (34). The black dot-dashed and dashed curves represent the improved mass functions P06 and YNY of equations (35) and (36), respectively.

## 6 CONCLUSIONS

In this work, we generalized the spherical collapse model in HDE cosmologies with time-varying EoS parameter  $w_{de}$ . The advantage of HDE models is that they are constructed on the basis of the holographic principle in quantum gravity scenario (Susskind 1995). We assumed two different phases of HDE model i.e. quintessence regime ( $c \geq 1$ ) and phantom regime ( $c < 1$ ). In the case of phantom regime, we adopted the constrained value for the model parameter  $c = 0.815$  obtained in Enqvist & Sloth (2004), Gong (2004), Huang & Gong (2004), Huang & Li (2004) and Li et al. (2009). We first investigated the growth of structures in linear regime and showed that the growth of density perturbations  $g(a)$  is slowed down in HDE models compared to the EdS and  $\Lambda$ CDM models due to a larger Hubble parameter. In particular, we showed that the growth factor in quintessence and phantom regimes falls behind the  $\Lambda$ CDM model (see Fig. 2). Therefore, to observe the same fluctuations at the present time, the perturbations should start growing earlier in HDE model than in a  $\Lambda$ CDM model. We then studied the non-linear phase of spherical collapse in HDE model. We obtained fitting formulas governing the correlation between turn-around redshift  $z_{ta}$  and virial redshift  $z_c$  in HDE cosmologies. At large enough redshifts, the effect of DE in HDE models on turn-around is negligible and  $z_{ta}$  approaches the value of the EdS Universe. Using the generalized virial condition obtained in time-varying HDE models, we obtained the characteristic parameter of spherical collapse model  $\delta_c$ ,  $\xi$  (the overdensity at turn-around redshift) and  $\Delta_{vir}$ . We showed that the overdense spherical region at the moment of turn-around are denser in HDE models than in  $\Lambda$ CDM and EdS models. It has been shown that in HDE models (both phantom and quintessence regimes), the virial overdensity  $\Delta_{vir}$  is larger than in the  $\Lambda$ CDM model. Hence, in a HDE Universe more concentrated structures can be formed compared to a  $\Lambda$ CDM model. Due to non-zero density at the outer layers of clusters during the virialization process, we studied the effect of a non-vanishing surface pressure on the parameters of the spherical collapse in HDE cosmologies and showed that in this case smaller virial radii and larger virial overdensities  $\Delta_{vir}$  can be achieved with respect to the case in which the surface pressure terms are neglected. We also predicted that for larger values of the holographic parameter  $c$ , the virial overdensity  $\Delta_{vir}$  is larger. We could put a limit on the holographic parameter  $c$ , based on the observational value of present-time virial overdensity  $\Delta_{vir}^{obs}(z_c = 0) = 348 \pm 73 (\pm 146)$

with  $1\sigma$  ( $2\sigma$ ) error bars calculated in Basilakos et al. (2010). We showed that the present-time virial overdensity in HDE cosmology has good agreement with observational value at  $2\sigma$  level for the holographic parameter  $c$  in the range of  $0.8 \leq c \leq 4.5$ . Finally, using the fitting formula proposed by Sheth & Tormen (Sheth & Tormen 1999, 2002) for the mass function, we obtained the mass function and number densities of clusters in HDE cosmologies. The number densities of small halo objects are the same for all models. However, we showed that the HDE models deviate from concordance  $\Lambda$ CDM model at high-mass halo objects. We showed that the ST mass functions in HDE cosmologies is smaller than the improved mass functions presented in del Popolo (2006a,b) and Yahagi et al. (2004) for all mass scales investigated.

## ACKNOWLEDGEMENTS

We would like to thank an anonymous referee for giving us constructive comments that helped us to improve the scientific content of the manuscript. FP is supported by STFC grant ST/H002774/1. TN and MM thank A. Mehrabi for useful discussions.

## REFERENCES

- Abramo L. R., Batista R. C., Liberato L., Rosenfeld R., 2007, *J. Cosmol. Astropart. Phys.*, 11, 12
- Afshordi N., Cen R., 2002, *ApJ*, 564, 669
- Alam U., Sahni V., Starobinsky A. A., 2004, *J. Cosmol. Astropart. Phys.*, 6, 8
- Allen S. W., Schmidt R. W., Ebeling H., Fabian A. C., van Speybroeck L., 2004, *MNRAS*, 353, 457
- Arzano M., Kephart T. W., Ng Y. J., 2007, *Phys. Lett. B*, 649, 243
- Ascasibar Y., Yepes G., Gottlöber S., Müller V., 2004, *MNRAS*, 352, 1109
- Avila-Reese V., Firmani C., Hernández X., 1998, *ApJ*, 505, 37
- Bamba K., Capozziello S., Nojiri S., Odintsov S. D., 2012, *Ap&SS*, 342, 155
- Barkana R., Loeb A., 2001, *Phys. Rep.*, 349, 125
- Bartelmann M., Doran M., Wetterich C., 2006, *A&A*, 454, 27
- Basilakos S., 2003, *ApJ*, 590, 636
- Basilakos S., Sanchez J. C. B., Perivolaropoulos L., 2009, *Phys. Rev. D*, 80, 043530
- Basilakos S., Plionis M., Solà J., 2010, *Phys. Rev. D*, 82, 083512
- Bernardeau F., 1994, *ApJ*, 433, 1
- Bertschinger E., 1985, *ApJS*, 58, 39
- Bond J. R., Cole S., Efstathiou G., Kaiser N., 1991, *ApJ*, 379, 440
- Brax P., Rosenfeld R., Steer D. A., 2010, *J. Cosmol. Astropart. Phys.*, 8, 033
- Bromm V., Yoshida N., 2011, *ARA&A*, 49, 373
- Carroll S. M., 2001, *Living Rev. Relativ.*, 380, 1
- Cataldo M., Cruz N., del Campo S., Lepe S., 2001, *Phys. Lett. B*, 509, 138
- Ciardi B., Ferrara A., 2005, *Space Sci. Rev.*, 116, 625
- Cohen A. G., Kaplan D. B., Nelson A. E., 1999, *Phys. Rev. Lett.*, 82, 4971
- Copeland E. J., Sami M., Tsujikawa S., 2006, *Int. J. Mod. Phys. D*, 15, 1753
- Crook A. C., Huchra J. P., Martimbeau N., Masters K. L., Jarrett T., Macri L. M., 2007, *ApJ*, 655, 790
- Debnath U., Nath S., Chakraborty S., 2006, *MNRAS*, 369, 1961
- del Popolo A., 2002, *MNRAS*, 336, 81
- del Popolo A., 2006a, *A&A*, 448, 439
- del Popolo A., 2006b, *ApJ*, 637, 12
- del Popolo A., Pace F., Lima J. A. S., 2013a, *Int. J. Mod. Phys. D*, 22, 1350038
- del Popolo A., Pace F., Lima J. A. S., 2013b, *Phys. Rev. D*, 87, 043527
- del Popolo A., Pace F., Lima J. A. S., 2013c, *MNRAS*, 430, 628
- Eisenstein D. J. et al., 2005, *ApJ*, 633, 560
- Eke V. R., Cole S., Frenk C. S., 1996, *MNRAS*, 282, 263
- Enqvist K., Sloth M. S., 2004, *Phys. Rev. Lett.*, 93, 221302
- Fillmore J. A., Goldreich P., 1984, *ApJ*, 281, 1

- Gong Y., 2004, *Phys. Rev. D*, 70, 064029  
Gong Y., 2005, *Class. Quantum Gravity*, 22, 2121  
Gong Y., Zhang Y. Z., 2005, *Phys. Rev. D*, 72, 043518  
Gunn J. E., Gott J. R., 1972, *ApJ*, 176, 1  
Guth A. H., 1981, *Phys. Rev. D*, 23, 347  
Ho S., Hirata C., Padmanabhan N., Seljak U., Bahcall N., 2008, *Phys. Rev. D*, 78, 043519  
Hoffman Y., Shaham J., 1985, *ApJ*, 297, 16  
Horellou C., Berge J., 2005, *MNRAS*, 360, 1393  
Hořava P., Minic D., 2000, *Phys. Rev. Lett.*, 85, 1610  
Hsu S. D. H., 2004, *Phys. Lett. B*, 594, 13  
Huang Q. G., Gong Y., 2004, *J. Cosmol. Astropart. Phys.*, 8, 006  
Huang Q. G., Li M., 2004, *J. Cosmol. Astropart. Phys.*, 8, 013  
Huterer D., Cooray A., 2005, *Phys. Rev. D*, 71, 023506  
Jaffe A. H. et al., 2001, *Phys. Rev. Lett.*, 86, 3475  
Jarosik N. et al., 2011, *ApJS*, 192, 14  
Komatsu E. et al., 2011, *ApJS*, 192, 18  
Kulinich Y., Novosyadlyj B., 2003, *J. Phys. Stud.*, 7, 234  
Lacey C., Cole S., 1993, *MNRAS*, 262, 627  
Lahav O., Lilje P. B., Primack J. R., Rees M. J., 1991, *MNRAS*, 251, 128  
Landau L. D., Lifshitz E. M., 1960, *Mechanics*. Pergamon Press, Oxford  
Li M., 2004, *Phys. Lett. B*, 603, 1  
Li M., Li X. D., Wang S., Zhang X., 2009, *J. Cosmol. Astropart. Phys.*, 6, 036  
Li M., Li X. D., Wang S., Wang Y., 2011, *Commun. Theor. Phys.*, 56, 525  
Lilje P. B., 1992, *ApJ*, 386, L33  
Linde A., 1990, *Phys. Lett. B*, 238, 160  
Lokas E. L., 2001, *Acta Phys. Pol. B*, 32, 3643  
Ma Y. Z., Gong Y., Chen X., 2009, *Eur. Phys. J. C*, 60, 303  
Meyer S., Pace F., Bartelmann M., 2012, *Phys. Rev. D*, 86, 103002  
Mota D. F., van de Bruck C., 2004, *A&A*, 421, 71  
Ng Y. J., 2001, *Phys. Rev. Lett.*, 86, 2946  
Ohta Y., Kayo I., Taruya A., 2003, *ApJ*, 589, 1  
Ohta Y., Kayo I., Taruya A., 2004, *ApJ*, 608, 647  
Pace F., Waizmann J. C., Bartelmann M., 2010, *MNRAS*, 406, 1865  
Pace F., Fedeli C., Moscardini L., Bartelmann M., 2012, *MNRAS*, 422, 1186  
Pace F., Moscardini L., Crittenden R., Bartelmann M., Pettorino V., 2014, *MNRAS*, 437, 547  
Padmanabhan T., 1996, *Cosmology and Astrophysics through Problems*. Cambridge Univ. Press, Cambridge  
Padmanabhan T., 2003, *Phys. Rep.*, 380, 235  
Papovich C. et al., 2010, *ApJ*, 716, 1503  
Pavón D., Zimdahl W., 2005, *Phys. Lett. B*, 628, 206  
Peacock J. A., 1999, *Cosmological Physics*. Cambridge Univ. Press, Cambridge  
Peebles P. J. E., 1993, *Principles of Physical Cosmology*. Princeton Univ. Press, Princeton, NJ  
Peebles P. J., Ratra B., 2003, *Rev. Mod. Phys.*, 75, 559  
Percival W. J., 2005, *A&A*, 443, 819  
Percival W. J. et al., 2010, *MNRAS*, 401, 2148  
Perlmutter S. et al., 1999, *ApJ*, 517, 565  
Planck Collaboration XV 2014, *A&A*, 571, A15  
Planck Collaboration XVI 2014, *A&A*, 571, A16  
Planck Collaboration XIX 2014, *A&A*, 571, A19  
Press W. H., Schechter P., 1974, *ApJ*, 187, 425  
Riess A. G. et al., 1998, *AJ*, 116, 1009  
Riess A. G. et al., 2004, *ApJ*, 607, 665  
Riess A. G. et al., 2007, *ApJ*, 659, 98  
Ryden B. S., Gunn J. E., 1987, *ApJ*, 318, 15  
Sahni V., Starobinsky A., 2000, *Int. J. Mod. Phys. D*, 9, 373  
Sheth R. K., Tormen G., 1999, *MNRAS*, 308, 119  
Sheth R. K., Tormen G., 2002, *MNRAS*, 329, 61  
Sheykhi A., 2011, *Phys. Rev. D*, 84, 107302  
Starobinsky A. A., 1980, *Phys. Lett. B*, 91, 99  
Subramanian K., Cen R., Ostriker J. P., 2000, *ApJ*, 538, 528  
Susskind L., 1995, *J. Math. Phys.*, 36, 6377  
Tegmark M. et al., 2004, *Phys. Rev. D*, 69, 103501  
Thomas S., 2002, *Phys. Rev. Lett.*, 89, 081301  
Viana P. T. P., Liddle A. R., 1996, *MNRAS*, 281, 323  
Vikhlinin A. et al., 2009, *ApJ*, 692, 1060  
Wang L., Steinhardt P. J., 1998, *ApJ*, 508, 483  
Wang Y., Tegmark M., 2005, *Phys. Rev. D*, 71, 103513  
Weinberg S., 1989, *Rev. Mod. Phys.*, 61, 1  
White S. D. M., Rees M. J., 1978, *MNRAS*, 183, 341  
Williams L. L. R., Babul A., Dalcanton J. J., 2004, *ApJ*, 604, 18  
Wu Q., Gong Y., Wang A., Alcaniz J. S., 2008, *Phys. Lett. B*, 659, 34  
Yahagi H., Nagashima M., Yoshii Y., 2004, *ApJ*, 605, 709  
Zhang X., Wu F. Q., 2005, *Phys. Rev. D*, 72, 043524  
Zhao G. B., Crittenden R. G., Pogosian L., Zhang X., 2012, *Phys. Rev. Lett.*, 109, 171301  
Zimdahl W., Pavón D., 2007, *Class. Quantum Gravity*, 24, 5461

This paper has been typeset from a  $\text{\TeX/L\AA\TeX}$  file prepared by the author.